TOWARDS CONTROLLING AND UNDERSTANDING NANOSTRAND NETWORK FORMATION AT THE AIR/WATER INTERFACE

Iryna I. Perepichka, Antonella Badia, and C. Geraldine Bazuin

Department of Chemistry, University of Montreal
C.P. 6128 succursale Centre-ville
Montreal (Quebec) H3C 3J7, Canada

Introduction

Many technological applications require thin films with well-ordered and well-defined nanopatterns. In materials science, block copolymers have particular interest because they can self-assemble to form periodic nanostructures. One of the more unusual patterns discovered in block copolymer monolayers prepared by the Langmuir-Blodgett (LB) technique is what we term the nanostrand network.[1–5] Films with this morphology might be used, for example, as a template to obtain nanowires by depositing metals or conjugated monomers for polymerization, or as a nanoseparation membrane following multilayer transfers. Here, we follow up on our initial discovery of the LB nanostrand network using poly(styrene)-poly(4-vinyl pyridine) (PS-P4VP) diblock copolymers complexed by hydrogen-bonding with 3-pentadecylphenol (PDP) (**Figure 1**).[1] We show, in particular, the molecular parameters and experimental conditions that allow the optimal formation of this morphology and new insights into its self-assembly mechanism. The PS-P4VP/PDP system was previously studied in the bulk giving 3-dimensional nanostructures,[6,7] in contrast to the present 2-dimensional nanostructures.

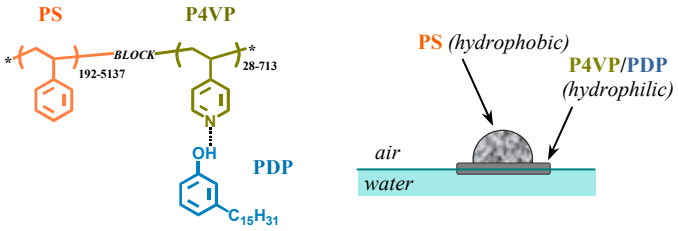

Figure 1. *Left*: complexes investigated, with range of block lengths in terms of number of repeat units indicated. *Right*: schematic representation of a PS-P4VP/PDP aggregate at the air/water interface.

Experimental

Materials. Block copolymers (BCs) of PS-P4VP with P4VP contents ranging from 8 to 49 wt% (see **Figure 1** for the block length ranges) were obtained from *Polymer Source*, and used as received. 3-*n*-Pentadecylphenol (PDP) (*Sigma-Aldrich,* 90%) was recrystallized twice from hexane. Chloroform (≥99.8%), 1,2-dichloroethane (99.8%), and 1,1,2,2-tetrachloroethane (≥98.0%) were used as spreading solvents. Water was purified using the Millipore Milli-Q system (18.2 MΩ cm).

Instrumentation. The Langmuir-Blodgett monolayer films were prepared using the *KSV 3000* Langmuir-Blodgett system with subphase temperature control. The film surface was imaged by atomic force microscopy (AFM) in tapping mode using a multimode AFM with a Nanoscope IIIa controller (*Digital Instruments*).

Langmuir-Blodgett (LB) film preparation. PS-P4VP was dissolved in $CHCl_3$, $C_2H_4Cl_2$, or $C_2H_2Cl_4$, and then the desired proportion of PDP was added, generally to have a small excess of PDP relative to the VP units (1.1–1.3 molar ratio). The obtained solution was diluted with the solvent to the desired concentration, and left to stir overnight at room temperature in a sealed vial. To obtain LB films, the solution was spread dropwise and evenly on the Milli-Q water surface (8°, 20°, or 38°C) in a clean Langmuir trough (150 x 518 mm). After a 20–60 min wait to ensure solvent evaporation, the barriers were compressed at a speed of 1–10 mm/min to the desired surface pressure (π=0.5–40 mN/m), followed by a 20–30 min period to stabilize the water subphase. Then, the film was transferred onto freshly cleaved mica previously immersed in the subphase by withdrawing it at a controlled rate (5–10 mm/min) through the monolayer at the water surface.

Results and Discussion

General principle of morphology formation. When spread on the water surface, the PS-P4VP/PDP solution forms a monolayer. Upon solvent evaporation, the hydrophobic PS block adopts a globular form to minimize interaction with the water surface, and the hydrophilic P4VP/PDP block spreads on the water surface in monolayer form below and around the PS globule (**Figure 1**). The PDP is considered to be H-bonded to the P4VP, with the alkyl chains most likely pointing away from the water surface.

Influence of block ratio on morphology. In general, depending on the relative block lengths of the block copolymer, different morphologies can be obtained.[8–10] In our case, the nanostrand network morphology is observed for P4VP weight fractions between ca. 10 and 20% (**Figure 2**) under the following conditions: total molecular weight of block copolymer ca. 50 000, spread from relatively concentrated $CHCl_3$ solution (1.5-2.0 mg/mL; see below) at 20 °C, transferred at a surface pressure of 5 mN/m. Below ca. 10%, planar aggregates of variable size, where the short P4VP blocks lie between the PS plane and the water phase, are formed. Above ca. 20%, the nanodot morphology, where the long P4VP/PDP blocks spread on the water surface around the PS globules thus isolating them from one another, is formed. More specifically, the nanostrand network morphology appears fully for 12 and 16% P4VP, whereas it is mixed with the planar aggregate morphology for 9% and with the nanodot morphology for 20%. The width and height of the strands is 60±10 and 5–6 nm, respectively. In the nanodot morphology, the dot height and spacing depended on the PS and P4VP block lengths, respectively (**Figure 3**). These data are consistent with what was observed by Zhu et al. for PS-P4VP where the P4VP block is quaternized by decyl iodide,[8] except that the strands tend to be much shorter than in our case.

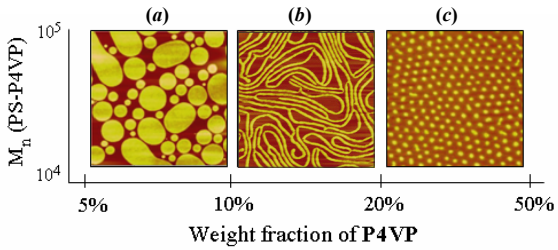

Figure 2. Representative AFM height images (area on the order of 3 x 3 μm) showing the dependence of the morphology on the weight fraction of the P4VP block: (*a*) planar aggregates, (*b*) nanostrands, (*c*) nanodots.

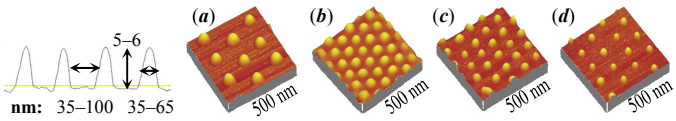

Figure 3. AFM images of LB monolayer films with the nanodot morphology: (*a*) PS_{398}-$P4VP_{166}$/PDP (wt_{P4VP}=30%); (*b*) PS_{316}-$P4VP_{76}$/PDP (wt_{P4VP}=20%); (*c*) PS_{306}-$P4VP_{126}$/PDP (wt_{P4VP}=29%); (*d*) PS_{192}-$P4VP_{181}$/PDP (wt_{P4VP}=49%).

Nanostrand network optimization. We investigated the system, PS_{384}-$P4VP_{53}$/PDP (weight fraction P4VP, 12%), under different experimental conditions, and found that they can strongly influence the morphology obtained. Thus, at low concentrations (0.1–0.35 mg/mL), nanodots and planar aggregates are predominant, while the nanostrand network is formed only when the solution concentration is relatively high (1.7–2.0 mg/mL). For the latter, the nanostrand network is obtained even at very low surface pressure (0.5–5 mN/m), whereas, for dilute solutions, nanostrands do not form even at high surface pressure. This can be explained by the need for sufficient density of BC material on the water surface to allow continuous strands to form, which must occur very rapidly after solution deposition. For low solution concentrations, only isolated aggregates can form due to depletion of matter, and after solvent evaporation, which is rapid, the morphology is frozen in, so that reorganization cannot take place at higher surface pressures even though the effective surface concentrations are higher.

Chloroform is the most common solvent used to prepare LB films, but if we assume that solvent is necessary to maintain mobility in the system,[1] it is of interest to turn to solvents that evaporate more slowly. To this end, we chose 1,2-dichloroethane and 1,1,2,2-tetrachloroethane, chemically similar to chloroform but possessing higher boiling points, 84 and 147°C, respectively, (61°C for $CHCl_3$). Use of these solvents in the high concentration regime did not change the morphology obtained, which is nanostrand in all cases. However, $C_2H_2Cl_4$ led to longer strands (fewer ends visible) with fewer branching points (**Figure 4*b***), even more so when the experiment was conducted at low temperature (**Figure 4*a***). On the other hand, high temperature gives irregular planar type aggregates (**Figure 4*c***) that might be explained by hydrogen bond breakage between VP and PDP, and possibly dissolution of PDP in PS.[7] This causes a reduction in the effective hydrophilic block fraction, placing the BC in the regime for planar aggregates.

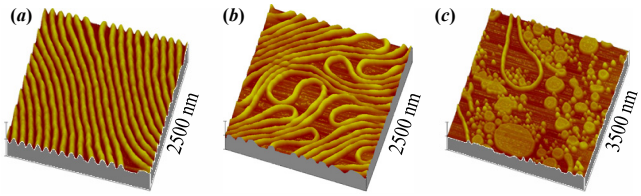

Figure 4. AFM height images obtained for PS_{384}-$P4VP_{53}$/PDP monolayer films spread from $C_2H_2Cl_4$ at: (*a*) 8°C, (*b*) 20°C, (*c*) 38°C.

Under optimal conditions, we have been able to obtain well-defined and reproducible nanostrand network morphology over very large surface areas (**Figure 5**). The strands tend to be highly aligned when using $C_2H_2Cl_4$ as spreading solvent and low deposition temperature. The strands are extremely long, more then 30 μm, which is 6 000 times greater then their height.

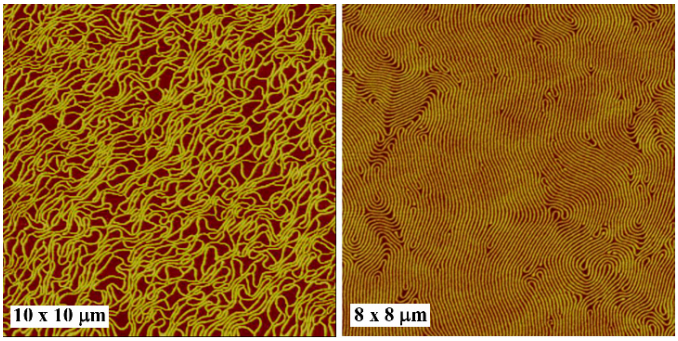

Figure 5. AFM height images of LB monolayer films of PS_{384}-$P4VP_{53}$/PDP spread from (*left*) $CHCl_3$ and (*right*) $C_2H_2Cl_4$ at 8°C (copolymer concentration 1.75 mg/mL, molar ratio VP:PDP=1:1.3).

Removal of complexed PDP. Following formation of the nanostrand network monolayer, the PDP was removed by soaking the film in acetone, an excellent solvent for PDP, for 10–30 minutes. This led to the pattern shown in **Figure 6**, showing strands that are composed of a series of essentially two parallel rows of triangularly arranged nanodots.

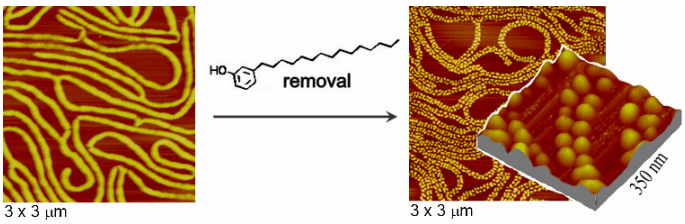

Figure 6. AFM images of the nanostrand network pattern (*left*) before and (*right*) after PDP is washed out by soaking the film in acetone.

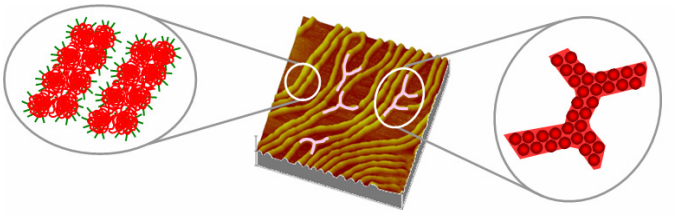

Figure 7. Schematic representation of the mechanism of nanostrand network formation.

Possible mechanism of nanostrand network formation. The morphology shown in **Figure 6** suggests that the continuity in the original nanostrands occurs via the PDP-complexed P4VP blocks, whereas the PS is coiled up in globules as in the nanodot morphology. This suggests that the nanostrands form by the mechanism shown schematically in **Figure 7**. Being in the regime where the cylindrical morphology is favored, the nanodot units self-assemble longitudinally at the air-water interface. Association in triangular format maintains close-packing of the nanodots in the nanostrands. Defects occur most commonly as a change in growth direction, which favors division of the strand into two. This corresponds to the experimental observation that the maximum number of strands radiating out from a common point is three. Termination of the strands occurs under conditions of depletion of matter during the self-assembly period, as indicated by the absence of nanostrand morphology for the more dilute spreading solutions. As the solvent evaporates, the blocks become rigid and the morphology then undergoes no further evolution. When mobility is retained for a sufficiently long time and in the absence of external perturbations (such as thermal energy), conditions which are met when spreading from tetrachloroethane at low temperatures, the nanostrands themselves self-assemble in as parallel a format as possible, as shown in **Figure 5**. This also leaves large areas in the LB monolayer with no visible matter present (not shown). In this connection, it is noteworthy that the distance of closest approach between two strands is twice the extended length of the P4VP block (like in the nanodot morphology), whereas the distance between two spheres within the strands is half that. This indicates that the P4VP chains within the strands are intertwined, whereas they do not interpenetrate between strands, which may be indicative of strand association occurring in a second step following strand formation.

Conclusions

We have investigated PS-P4VP/PDP self-assembly at the air-water interface, and presented different factors influencing the 2D morphologies obtained. Optimization of the material composition and experimental conditions allows us to fabricate highly reproducible monolayers with well-defined nanostrand network morphology over large areas. Subsequent removal of PDP reveals a nanodot substructure in the nanostrands, leading us to propose a possible mechanism of nanostrand network formation.

Acknowledgements. The authors are members of the Centre for Self-Assembled Chemical Structures (CSACS). The research was funded by NSERC (Canada). IIP also acknowledges FQRNT (Quebec) for a Merit Scholarship for foreign students (2007–2010) and Université de Montréal for financial support.

References

(1) Lu, Q.; Bazuin, C.G. *Nano Lett.* **2005**, *5*, 1309.
(2) Devereaux, C.A.; Baker, S.M. *Macromolecules* **2002**, *35*, 1921.
(3) Seo, Y.-S.; Kim, K.S.; Galambos, A.; Lammertink, R.G.H.; Vancso, G.J.; Sokolov, J.; Rafailovich, M. *Nano Lett.* **2004**, *4*, 483.
(4) Cheyne, R.; Moffitt, M.G. *Langmuir* **2006**, *22*, 8387.
(5) Price, E.W.; Guo, Y.; Wang, C.-W.; Moffitt, M.G. *Langmuir* **2009**, *25*, 6398.
(6) Ruokolainen, J.; Saariaho, M.; Ikkala, O.; ten Brinke, G.; Thomas, E.L.; Torkkeli, M.; Serimaa, R. *Macromolecules* **1999**, *32*, 1152.
(7) Valkama, S.; Ruotsalainen, T.; Nykänen, A.; Laiho, A.; Kosonen, H.; ten Brinke, G.; Ikkala, O.; Ruokolainen, J. *Macromolecules* **2006**, *39*, 9327.
(8) Zhu, J.; Eisenberg, A.; Lennox, R.B. *Macromolecules* **1992**, *25*, 6547.
(9) Förster S.; Plantenberg, T. *Angew. Chem. Int. Ed.* **2002**, *41*, 688.
(10) Gunawidjaja, R.; Peleshanko, S.; Genson, K.L.; Tsitsilianis, C.; Tsukruk, V.V. *Langmuir* **2006**, *22*, 6168.